

Frequency shifts of high-order harmonics from ZnO crystals by chirped laser pulses

Yu Zhao(赵宇), Xiao-Jin Liu(刘晓瑾), Shuang Wang(王爽), Xiao-Xin Huo(霍晓鑫), Yun-He Xing(邢云鹤), and Jun Zhang(张军)

Citation: Chin. Phys. B, 2025, 34 (**3**): 033201. DOI: 10.1088/1674-1056/ada9dc
Journal homepage: http://cpb.iphy.ac.cn; http://iopscience.iop.org/cpb

What follows is a list of articles you may be interested in

Electron correlation in two-electron atoms: A Bohmian analysis of high-order harmonic generation in high-frequency domain

Yang Song(宋阳), Shu Han(韩姝), Yujun Yang(杨玉军), and Fuming Guo(郭福明)
Chin. Phys. B, 2024, 33 (**12**): 123201. DOI: 10.1088/1674-1056/ad84d1

Interference of harmonics emitted by different tunneling momentum channels in laser fields

Ling-Yu Zhang(张玲玉), Zhuo-Xuan Xie(谢卓璇), Can Wang(王灿), Xin-Lei Ge(葛鑫磊), and Jing Guo(郭静)
Chin. Phys. B, 2024, 33 (**9**): 093201. DOI: 10.1088/1674-1056/ad5d95

Role of excited states in helium-like ions on high-order harmonic generation

Jiang-Hua Luo(罗江华) and Jia-Jun Xiao(肖佳俊)
Chin. Phys. B, 2023, 32 (**11**): 113201. DOI: 10.1088/1674-1056/ace317

Phase-coherence dynamics of frequency-comb emission via high-order harmonic generation in few-cycle pulse trains

Chang-Tong Liang(梁畅通), Jing-Jing Zhang(张晶晶), and Peng-Cheng Li(李鹏程)
Chin. Phys. B, 2023, 32 (**3**): 033201. DOI: 10.1088/1674-1056/acac0f

High-order harmonic generation of the cyclo[18]carbon molecule irradiated by circularly polarized laser pulse

Shu-Shan Zhou(周书山), Yu-Jun Yang(杨玉军), Yang Yang(杨扬), Ming-Yue Suo(索明月), Dong-Yuan Li(李东垣), Yue Qiao(乔月), Hai-Ying Yuan(袁海颖), Wen-Di Lan(蓝文迪), and Mu-Hong Hu(胡木宏)
Chin. Phys. B, 2023, 32 (**1**): 013201. DOI: 10.1088/1674-1056/aca3a1

Frequency shifts of high-order harmonics from ZnO crystals by chirped laser pulses

Yu Zhao(赵宇)[1], Xiao-Jin Liu(刘晓瑾)[1], Shuang Wang(王爽)[1], Xiao-Xin Huo(霍晓鑫)[2], Yun-He Xing(邢云鹤)[1], and Jun Zhang(张军)[1,†]

[1] *Institute of Atomic and Molecular Physics, Jilin University, Changchun* 130012, *China*
[2] *School of Science, Shenyang Ligong University, Shenyang* 110159, *China*

(Received 13 November 2024; revised manuscript received 30 December 2024; accepted manuscript online 14 January 2025)

We investigate theoretically the effects of chirped laser pulses on high-order harmonic generation (HHG) from solids. We find that the harmonic spectra display redshifts for the driving laser pulses with negative chirp and blueshifts for those with positive chirp, which is due to the change in the instantaneous frequency of the driving laser for different chirped pulses. The analysis of crystal-momentum-resolved ($\boldsymbol{k}$-resolved) HHG reveals that the frequency shifts are equal for the harmonics generated by different crystal momentum channels. The frequency shifts in the cutoff region are larger than those in the plateau region. With the increase of the absolute value of the chirp parameters, the frequency shifts of HHG become more significant, leading to the shifts from odd- to even-order harmonics. We also demonstrate that the frequency shifts of harmonic spectra are related to the duration of the chirped laser field, but are insensitive to the laser intensity and dephasing time.

Keywords: high-order harmonic generation, ZnO crystal, chirped laser pulse, spectral shift

PACS: 32.80.Rm, 42.65.Ky, 42.65.Re

DOI: 10.1088/1674-1056/ada9dc **CSTR:** 32038.14.CPB.ada9dc

1. Introduction

High-order harmonic generation (HHG) from gas-phase atoms and molecules has opened up a new frontier in ultrafast science,[1–4] which makes it possible to generate attosecond pulses and the measurement with attosecond temporal.[3] The temporal characteristics of HHG have positioned it as a unique tool for exploring time-resolved spectroscopy[5] and probing electron dynamics.[6–8] Solid systems possess more intricate structures and dynamical processes compared to gas systems, including natural crystal orientation,[9,10] high electron density,[11] and periodic structure.[12–14] Consequently, the HHG in solid exhibits intriguing behaviors that are absent in gases. For instance, the cutoff energies of harmonics in ZnO exhibit a linear dependence on the driving field strength.[7] This finding differs from the cutoff law predicted by the gas three-step model, which states that the cutoff energy is proportional to the square of the field strength.[2] Due to the advancements in long-wavelength laser pulses, the solid HHG has received a great deal of attention, promising to be novel spectroscopic tools.[15]

The laser waveform has a significant effect in all laser-matter interaction processes. In experiment, the chirped pulses can be generated by manipulating the space between two gratings of the laser compressor.[16] Popovici *et al.*[16] demonstrated the effects of the pump laser chirp on frequency shifts of the harmonics from over-dense plasmas experimentally. The harmonic spectra present a blueshift for driving laser pulses with negative chirp, whereas it undergoes a redshift for those with positive chirp. While, they found that adding chirp to the pump laser led to a decrease in harmonic efficiency. Aiming to achieve enhanced harmonic efficiency[17,18] and generate the isolated attosecond pulses (IAPs),[19–22] many investigations have been devoted to the effects of the chirp of laser pulses on their interactions with matter. By a small positive chirp, Qiao *et al.*[18] theoretically investigated the enhancement of HHG intensity near the cutoff region of hydrogen (H) atom. Using chirped laser pulses, Du *et al.*[23] effectively improved the high-order harmonic efficiency of the second plateau by increasing the populations of the high-lying conduction band (CB). The laser chirp effect on the solid HHG spectra has been investigated by solving the time-dependent Schrödinger equation (TDSE). It revealed that a frequency shift is observed within the first plateau. In 2019, by optimizing the waveform of the two-color chirped laser pulses, a "temporal gate" approach has been proposed to produce an IAP by simultaneously improving the conversion efficiency for the HHG, as reported by He *et al.*[24]

The physical mechanism behind the frequency shift of HHG spectra has been increasingly investigated both experimentally and theoretically.[25–27] The spectral redshift in HHG

†Corresponding author. E-mail: junzhang@jlu.edu.cn

© 2025 Chinese Physical Society and IOP Publishing Ltd. All rights, including for text and data mining, AI training, and similar technologies, are reserved.

emitted by the H_2^+ molecule is attributed to a decrease of the ionization energy, occurring between the recombination time and ionization time.[25] The delayed enhanced ionization resulting from the enhanced excitation has led to the spectral redshift, within high-intensity and ultrashort laser pulses.[26] In addition, the nonadiabatic spectral redshift in both atomic and solid systems has extensively investigated, which is due to the high-order harmonics generated predominantly on the falling part of the laser pulse.[28,29]

In this work, we investigate the frequency shift of HHG from ZnO solids driven by the chirped laser pulses. For the different chirp parameters, the harmonic spectra are red-shifted or blue-shifted, which is due to the shift in the instantaneous frequency of the diving laser field. By illustrating the crystal-momentum-resolved harmonics, we show the frequency shifts of the harmonics generated by each crystal momentum channel. Moreover, we also investigate the frequency shifts of the HHG under different pulse durations to further explain the underlying physical mechanism.

2. Method

In our simulations, the electronic transition mainly occurs in the highest valence band (VB) and the lowest CB. Thus, we investigate the HHG in ZnO crystals by solving the two-band semiconductor Bloch equations (SBEs),[30–32] which can be written as follows (atomic units are used in this paper unless stated otherwise):

$$\dot{n}_m = \mathrm{i}\sum_{m'\neq m}\Omega_{mm'}\pi_{mm'}\,\mathrm{e}^{\mathrm{i}S_{mm'}}+\mathrm{c.c.}, \tag{1}$$

$$\begin{aligned}\dot{\pi}_{mm'} = &-\frac{\pi_{mm'}}{T_2}+\mathrm{i}\Omega^*_{mm'}\left(n_m-n_{m'}\right)\mathrm{e}^{-\mathrm{i}S_{mm'}}\\&+\mathrm{i}\sum_{m''\notin\{m,m'\}}\left(\Omega_{m'm''}\pi_{mm''}\,\mathrm{e}^{\mathrm{i}S_{m'm''}}\right.\\&\left.-\Omega^*_{mm''}\pi^*_{m'm''}\,\mathrm{e}^{-\mathrm{i}S_{mm''}}\right),\end{aligned} \tag{2}$$

where $n_m(\boldsymbol{K},t)$ represents the population of electron on VB or CB. $m=v$ stands for the VB and $m=c$ stands for the CB. $\Omega_{mm'}(\boldsymbol{K},t)=E(t)\cdot\boldsymbol{d}_{mm'}[\boldsymbol{K}+\boldsymbol{A}(t)]$ is the Rabi frequency. The initial crystal momentum $\boldsymbol{k}$ can be transformed to a moving momentum frame by Bloch acceleration theorem as $\boldsymbol{k}=\boldsymbol{K}+\boldsymbol{A}(t)$. Thus, the first Brillioun zone (BZ) is also shifted to $\overline{\mathrm{BZ}}=\mathrm{BZ}-\boldsymbol{A}(t)$. $\boldsymbol{d}_{mm'}[\boldsymbol{K}+\boldsymbol{A}(t)]$ is the transition dipole moment, which is dependent on the crystal momentum. $\pi_{mm'}(\boldsymbol{K},t)$ is the strength of polarization arising from the quantum coherence between the CB and VB. The expression

$$S_{mm'}(\boldsymbol{K},t)=\int_{-\infty}^{t}\varepsilon_{mm'}\left[\boldsymbol{K}+\boldsymbol{A}\left(t'\right)\right]\mathrm{d}t'$$

is defined as the classical action, with $\varepsilon_{mm'}=(E_m-E_{m'})$. T_2 is a dephasing time term, describing the coherence between the VB and CB.

The intraband current and interband current generated during this process can be obtained by[31–33]

$$\boldsymbol{j}_{\mathrm{ra}}(t)=\sum_m\int_{\overline{\mathrm{BZ}}}\boldsymbol{v}_m[\boldsymbol{K}+\boldsymbol{A}(t)]\,n_m(\boldsymbol{K},t)\,\mathrm{d}\boldsymbol{K}, \tag{3}$$

$$\boldsymbol{j}_{\mathrm{er}}(t)=\frac{\mathrm{d}}{\mathrm{d}t}\sum_{m\neq m'}\int_{\overline{\mathrm{BZ}}}\boldsymbol{p}_{mm'}(\boldsymbol{K},t)\,\mathrm{d}\boldsymbol{K}, \tag{4}$$

where $\boldsymbol{v}_m(\boldsymbol{k})=\nabla_{\boldsymbol{k}}E_m(\boldsymbol{k})$ is the band velocity of the electron (hole) on the CB (VB). $E_m(\boldsymbol{k})$ stands for the band dispersion. $\boldsymbol{p}_{mm'}(\boldsymbol{K},t)$ is the polarization, which can be written as

$$\boldsymbol{p}_{mm'}(\boldsymbol{K},t)=\boldsymbol{d}_{mm'}\pi_{mm'}(\boldsymbol{K},t)\,\mathrm{e}^{\mathrm{i}S_{mm'}}+\mathrm{c.c.} \tag{5}$$

The total HHG spectrum is then given by the Fourier transform of the total current

$$I_{\mathrm{HHG}}(\omega)=\omega^2\left|\int\left[\boldsymbol{j}_{\mathrm{ra}}(t)+\boldsymbol{j}_{\mathrm{er}}(t)\right]\mathrm{e}^{-\mathrm{i}\omega t}\,\mathrm{d}t\right|^2. \tag{6}$$

The laser electric field $E(t)$ is defined as follows:

$$E(t)=E_0 f(t)\cos\left[\omega_0 t+\delta(t)\right], \tag{7}$$

where $f(t)=\cos^2(\pi t/T)$ is the envelope function. $E_0=0.0035$ a.u. and $\omega_0=0.014$ a.u. are the peak amplitude and the central frequency of the laser pulse. T is the total duration of the laser pulse. $\delta(t)=\beta\tanh(t/T)$ is the chirp function and β is the chirp parameter.[34,35] When $\beta>0$, it represents a positive chirp. When $\beta<0$, it represents a negative chirp. In our one-dimensional (1D) SBE simulations, the parameters of the band structure of ZnO are taken from Ref. [36]. The polarization direction of the laser pulse is along the Γ–M direction of the BZ. The dipole elements are calculated by Eq. (7) in Ref. [37]. For the model ZnO crystal, the band dispersion and the momentum-resolved transition dipole have inversion symmetry along the Γ–M direction, the Berry connections and Berry curvatures are neglected in the 1D calculations.[38]

3. Results and discussion

Figure 1(a1) shows the linearly polarized laser electric fields with chirp parameters $\beta=-6$, 0, and 6, respectively. Compared with the chirp-free laser ($\beta=0$), the electric field near the maximum peak almost remains unchanged for $\beta=-6$ and 6, as shown in Fig. 1(a2). Moreover, we can see that when $\beta=-6$ or 6, the frequency of the laser field decreases or increases in comparison to the case of $\beta=0$. Figures 1(b1)–1(b2) show the temporal evolution of the vector potential

$$\boldsymbol{A}(t)=-\int_{-\infty}^{t}E\left(t'\right)\mathrm{d}t'.$$

For $\beta=0$ (green solid line), we can see that when the electric field reaches its extrema, the vector potential equals 0. The

same situations can also be seen for chirp parameters $\beta = -6$ (red dotted line) and 6 (blue dashed line). Besides, the values of the maximum vector potential for the chirped laser field with both the $\beta = 0$ and -6 are much higher than that of $\beta = 6$, and the maximum vector potential of $\beta = -6$ is the strongest.

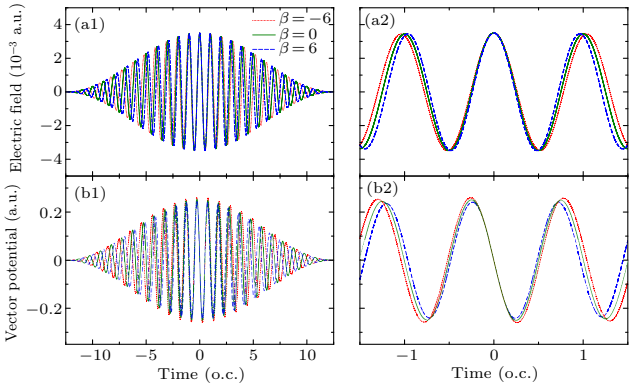


Fig. 1. (a1) Electric fields of the chirped laser pulses for the chirp parameters $\beta = -6$ (red dotted line), $\beta = 0$ (green solid line), and $\beta = 6$ (blue dashed line). The peak electric field, the wavelength and the duration are set as $E_0 = 0.0035$ a.u., $\lambda = 3255$ nm, and $T = 25$ o.c. (b1) The corresponding vector potentials of the chirped laser pulses in Fig. 1(a1). Panels (a2) and (b2) show the expanded view of panels (a1) and (b1) in the region of time from -1.5 o.c. to 1.5 o.c. (o.c. is short for optical cycle).

Figure 2 shows the harmonic spectra driven by the chirped laser pulses with $\beta = -6$, 0, and 6, respectively. One can see that the harmonic intensities are comparable with different chirp parameters, which is different from the decrease and increase of harmonic efficiencies by the chirped laser pulses as demonstrated in Refs. [16,23,39]. The electrons are initially excited from the VB to the CB driven by the intense laser field in this HHG process. The time-dependent population in the CB is related to the harmonic intensity in the solid. For example, Song *et al.*[40] showed that the larger the population in the CB, the higher the intensities of harmonics. In the inset of Fig. 2, we show the corresponding time-dependent CB populations. Clearly, the populations for these three different laser pulses are almost equal, which is in agreement with the harmonic intensities as shown in Fig. 2. The global spectral feature does not change with the chirped pulse, as expected, since the spectral is achieved by employing laser pulses with a small chirp. The laser intensities near the peak of the laser pulses are almost unchanged relative to the chirp-free field (see Fig. 1). While, the peak valley ratios of the harmonic spectrum have been decreased for $\beta = -6$ and $\beta = 6$ compared with the case of $\beta = 0$, especially in the high energy region. The peak valley ratios of HHG are come from the interferences of different quantum paths. Thus, our results reveal that the electron dynamics in HHG processes have been changed by using the chirped laser pulse, which results in the change of the peak valley ratio of the harmonic spectrum.[41] When the chirp parameter $\beta = 0$ (black solid line), the harmonic spectrum displays odd-order harmonics, attributing to the time translation symmetry and inversion symmetry about the Γ point.[31] When the chirp parameter $\beta = -6$ (red dotted line), it is found that the HHG spectrum is redshifted. The redshift increases in the higher-order harmonics and even-order harmonics are exhibited around the cutoff. The similar redshifts in the emission of HHG from solids in short laser pulses have also been demonstrated in Ref. [26]. The delayed population of higher CB leads to the delay of HHG emission. Most of HHG emissions occur in the falling edge of the laser pulse, which results in the redshifts of HHG in the second and third plateaus. They also illustrated that the redshifts vanish by using a two-band model, suggesting that the redshifts are attributed to the indirect multi-band transitions in the HHG process. It is expected that a different mechanism of harmonic radiation may be responsible for these redshifts in our two-band model. When the chirp parameter $\beta = 6$ (blue dashed line), the blueshifts of harmonics appear and increase in the higher-order harmonics, which is similar to that of $\beta = -6$ (red dotted line).

The interferences between harmonics generated by different crystal momentum channels play a key role in the total HHG spectrum, as demonstrated in Refs. [33,42,43]. Thus, we pay attention to the contributions of the HHG from different initial crystal momenta in the entire first BZ. To reveal the characteristics of spectral shift diving by the chirped laser pulse, we investigate the HHG generated by each $\boldsymbol{k}$ channel in the first BZ. The BZ is sampled using 401 $\boldsymbol{k}$ points that are evenly spaced in $[-\pi/a, \pi/a]$. The lattice constant a is set to 5.32 in the Γ–M direction.[33] Figures 3(a1)–3(a3) and 3(b1)–3(b3) display the intra- and interband harmonics as a function of the crystal momentum $\boldsymbol{k}$, respectively. In Fig. 3(a2) ($\beta = 0$), all $\boldsymbol{k}$ channels exhibit both odd- and even-order harmonics, with the exception of the $\boldsymbol{k} = 0$ (Γ point) channel and $\boldsymbol{k} = \pm 200$ (right-hand and left-hand edges of the first BZ) channels, which exhibit only odd-order harmonics.[31,33] In Fig. 3(a1) ($\beta = -6$), we can see a redshift in the $\boldsymbol{k}$-resolved harmonic spectra and the shifts are equal for each $\boldsymbol{k}$ channel. In Fig. 3(a3) ($\beta = 6$), a similar blueshift in the $\boldsymbol{k}$-resolved harmonic spectra can be seen.

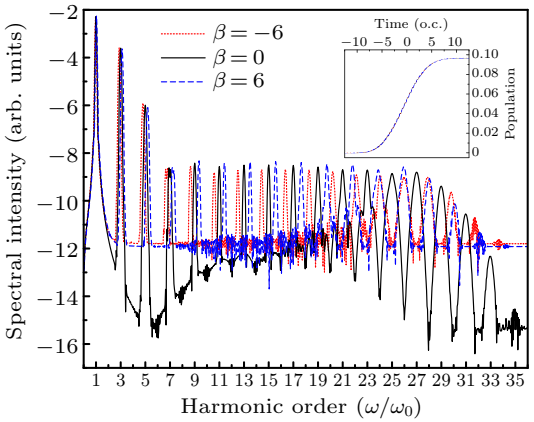


Fig. 2. Harmonic spectra produced by ZnO exposed to the chirped laser fields for $T_2 = (1/8)T_0$, using the same laser parameters as in Fig. 1(a1). $T_0 = 2\pi/\omega_0$ represents an optical cycle (o.c.). The inset of Fig. 2 shows the corresponding CB populations.

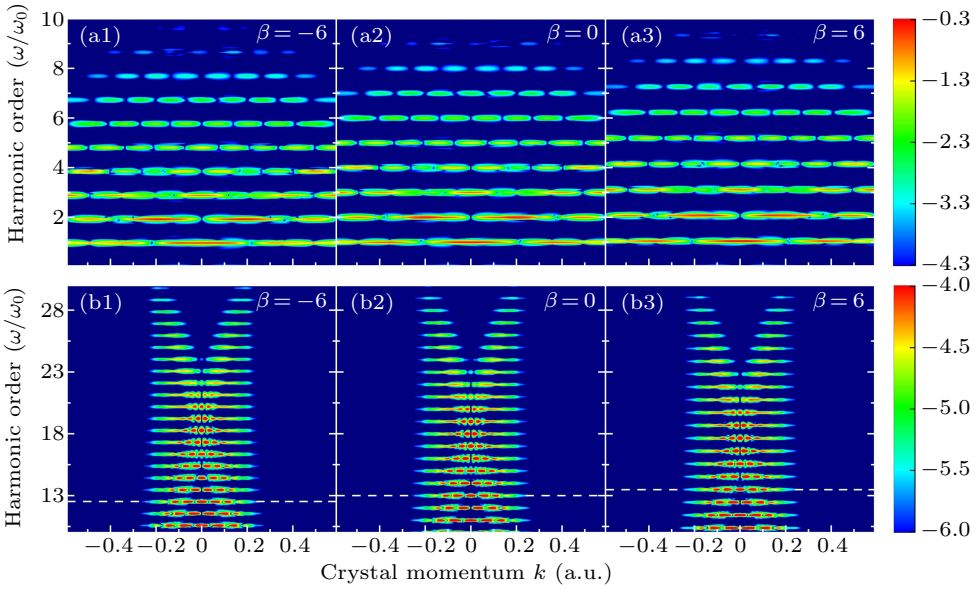


Fig. 3. The $\boldsymbol{k}$-resolved profiles of HHG from ZnO with different chirp parameters: (a1)–(a3) intraband harmonic spectra, (b1)–(b3) interband harmonic spectra. The horizontal white dashed lines indicate the 13th order harmonic. The other laser parameters are the same as those in Fig. 2.

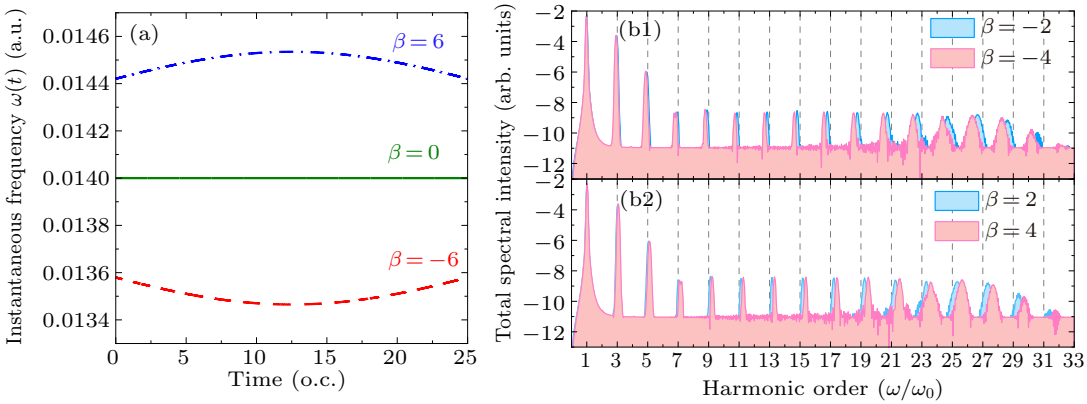


Fig. 4. (a) Temporal evolution of the instantaneous frequency $\omega(t)$ for the chirped laser pulses with $\beta = -6$ (red dashed line), $\beta = 0$ (green solid line), and $\beta = 6$ (blue doted-dashed line). (b) Harmonic spectra of ZnO driven by the chirped laser pulse with other chirp parameters. The other laser parameters are the same as those in Fig. 2.

Figures 3(b1)–3(b3) display the $\boldsymbol{k}$-resolved interband harmonic spectra, with the V-shaped cutoff energy. Taking the 13th order (the horizontal white dashed lines) as an example, it can be observed that a redshift or blueshift occurs when $\beta = -6$ or $\beta = 6$, and the shifts in the harmonic spectra are also equal for each $\boldsymbol{k}$ channel. Moreover, the shift of interband harmonics is larger than that of the intraband harmonics. We know that the interferences between harmonics generated by different $\boldsymbol{k}$ channels play a key role in the fine structure of the harmonic spectra.[33] However, the frequency shift of the $\boldsymbol{k}$-resolved harmonic spectra is consistent with the total harmonic spectra (see Fig. 2), integrated over the first BZ. That is, the chirp parameters of the driving pulse result in the frequency shifts of the HHG from different $\boldsymbol{k}$ channels equally, and the frequency shifts are equal to the corresponding total HHG spectrum. Thus, the interference between harmonics generated from different $\boldsymbol{k}$ channels has no significant effect on the frequency shift of the harmonic spectra. The frequency shift of the harmonic spectra is attributed to a different physical mechanism. This finding can help us probe the ultrafast electron-hole dynamics for solid HHG processes.

To elucidate the physical mechanism of the frequency shift observed in the harmonic spectra, we will show a more detailed characterization of the driving laser pulses. For the chirped pulses, the instantaneous angular frequency can be obtained by[16,25,35]

$$\omega(t) = \omega_0 + \frac{\mathrm{d}\delta(t)}{\mathrm{d}t} = \omega_0 + \frac{\beta}{T}\left[1 - \tanh^2\left(\frac{t}{T}\right)\right]. \quad (8)$$

In Fig. 4(a), we show the instantaneous frequencys of the chirped laser pulses as a function of time. For $\beta = -6$, the instantaneous frequency first decreases and then increases, reaching its minimum value at $t = 0$ o.c., which corresponds to the maximum peak of the driving laser pulse. While for $\beta = 6$, the instantaneous frequency first increases and then decreases, reaching its maximum value at $t = 0$ o.c. The harmonic order is inversely proportional to the frequency of the driving laser

pulse. Thus, the decrease in instantaneous frequency ($\beta = -6$) leads to a redshift of the harmonic spectra, while the increase in instantaneous frequency ($\beta = 6$) results in a blueshift of the harmonic spectra. These results are also in good agreement with the experimental studies from various solid surfaces.[16] In Figs. 4(b1) and 4(b2), we show the HHG spectra driven by the chirped laser pulse with different chirp parameters. We can see that the frequency shift of the harmonic spectra increases with the increase of the absolute value of β. By changing the chirp parameter, we can manipulate the frequency shifts of the HHG continuously, leading to the shifts from odd- to even-order harmonics. From Eq. (8), it is found that when the absolute value of β increases, the difference between the center frequency and instantaneous frequency of the laser pulse also increases, which results in a larger spectral redshift or blueshift. These results further demonstrate that the spectral shift is due to the change in the instantaneous frequency of the driving laser pulse. The similar frequency shifts of the harmonics have been observed in HHG from over-dense plasmas in experiments. They also illustrated that the frequency of the harmonic is proportional to the laser frequency at the maximum intensity of the chirped laser pulse.[16] In our work, we verify the effect of instantaneous frequency on the frequency shifts of HHG from ZnO solids through solving the two-band SBEs. Our results might pave an accessible route toward characterizing the chirp of the driving laser pulse.

In Fig. 5(a), we show the frequencies of the 21st (blue lines), 23rd (green lines), and 25th (red lines) harmonics as a function of the effective pulse duration for different chirp parameters. When $T = 25$ o.c., these three harmonics present redshifts with $\beta = -6$ (square symbols) and blueshifts for those with $\beta = 6$ (triangle symbols), and no obvious shift appears with $\beta = 0$ (circle symbols). When we decrease the laser pulse duration from $T = 25$ o.c. to 9 o.c., as shown in Fig. 5(a), the spectral redshift and blueshift gradually increase, which are in agreement with that illustrated from polar molecules.[44] In Ref. [44], it has been demonstrated that the harmonic emission is gradually shifted from the falling part to the rising part of the pulse when the pulse duration increases, which results in the spectral shift gradually decreasing.

In Figs. 5(b1) and 5(b2), we also show the instantaneous frequency of the chirped laser pulses as a function of time for $T = 9$ o.c. and 25 o.c., respectively. We find that the change in the instantaneous frequency gradually decreases as the laser pulse duration increases. For a short laser pulse [e.g., $T = 9$ o.c. as shown in Fig. 5(b1)], the range of change in the instantaneous frequency is more sensitive than the case of Fig. 5(b2). As shown in Fig. 5(b2), the difference between the center frequency and instantaneous frequency of the driving laser pulse is small. It has been demonstrated that the change in instantaneous frequency $\omega(t)$ decreases when the pulse duration increases, which results in the spectral shift gradually decreasing.

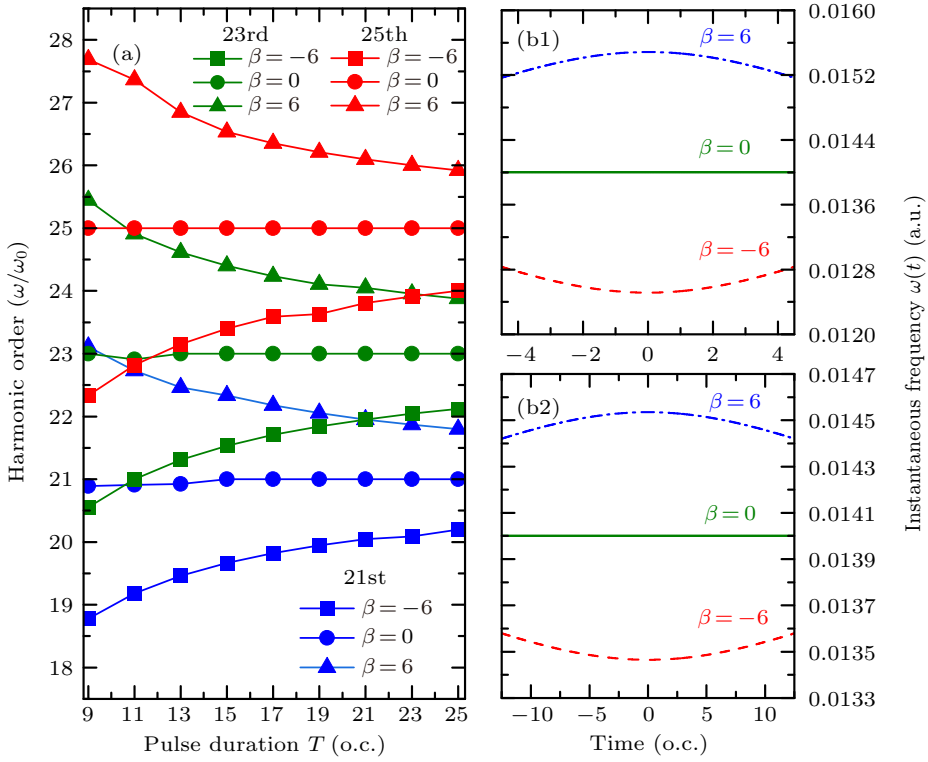


Fig. 5. (a) Spectral variation of the 21st, 23rd, and 25th harmonics for different pulse durations. (b1) and (b2) Temporal evolution of the instantaneous frequency $\omega(t)$ driven by the chirped laser pulses for $T = 9$ o.c. and $T = 25$ o.c. The other laser parameters are the same as those in Fig. 2.

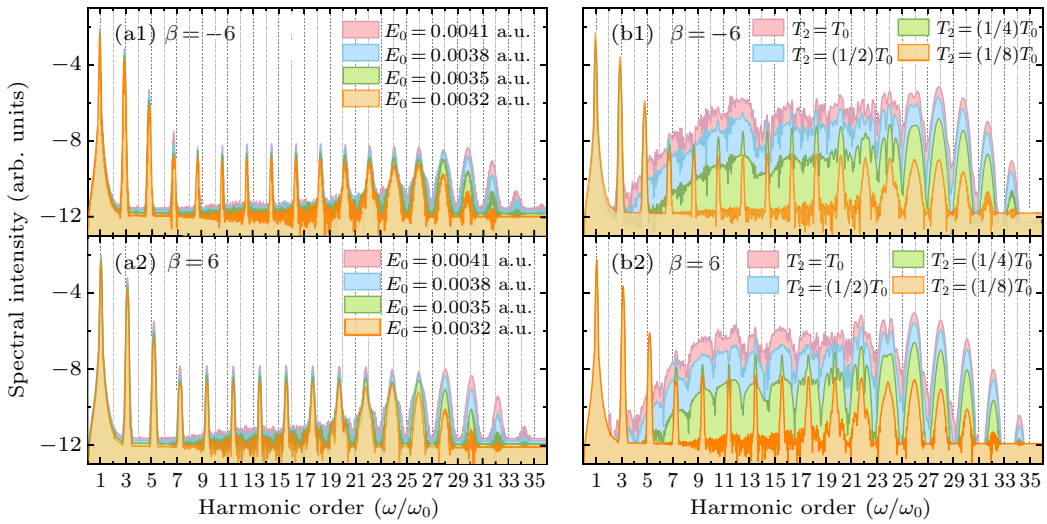


Fig. 6. Effects of the peak amplitude E_0 on the harmonic spectra for the different chirp parameters (a1) $\beta=-6$ and (b1) $\beta=6$. Effects of the dephasing time T_2 on the harmonic spectra for the different chirp parameters (a2) $\beta=-6$ and (b2) $\beta=6$. The other laser parameters are the same as those in Fig. 2.

For solid systems, it has been proved that the HHG is sensitive to the change of laser electric field intensity.[7,45] Therefore, we further study the effect of peak amplitude on frequency shifts. Figure 6(a1) presents the harmonic spectra driven by the chirped laser pulses with $\beta=-6$ for the different peak amplitudes E_0. It can be seen that with the increase of peak amplitude, the harmonic intensity can be enhanced, but the frequency shifts of the harmonic keep unchanged. A similar phenomenon can be seen in the harmonic spectra driven by the chirped laser pulses with $\beta=6$ as shown in Fig. 6(b1). Our findings differ from those presented in Ref. [25], which demonstrate that changes of peak amplitudes can affect the nuclear motion, ultimately impacting the frequency shift of the harmonic spectrum. We also investigate the effect of dephasing time on the frequency shift. As shown in Figs. 6(a2) and 6(b2), we can see that the increase of the dephasing time T_2 results in more modulations and some subpeak structures in HHG. However, the frequency shifts of the harmonic spectra are not affected.

4. Conclusion

In summary, we have investigated the spectral structure of solid HHG driven by the chirped laser pulses. We show that the harmonic intensities are almost unchanged for the chirped pulses with different chirp parameters, which is in agreement with the populations in the CB. Our results also show that the harmonic exhibits equal frequency shift for each $\boldsymbol{k}$ channel in the first BZ by analyzing the $\boldsymbol{k}$-resolved harmonic spectra. For the chirped laser pulses, the instantaneous frequency of the laser pulse changes as a function of time, which makes the harmonic spectra redshifted with negative chirp and blueshifted for those with positive chirp. Since the change of the instantaneous frequency at the center of the pulse is large, the frequency shifts in the cutoff region are larger than the shifts in the plateau region. The frequency shifts of the harmonic spectra depend on the selection of the duration time of the laser pulse, which can be explained by the instantaneous frequency. Furthermore, we find that the frequency shifts are insensitive to the variation of the peak amplitude and the dephasing time. We expect that our work can help to gain insight into the emission of solid HHG.

Acknowledgements

Project supported by the Natural Science Foundation of Jilin Province of China (Grant No. 20230101014JC) and the National Natural Science Foundation of China (Grant No. 12374265).

References

[1] L'Huillier A and Balcou P 1993 *Phys. Rev. Lett.* **70** 774
[2] Corkum P B 1994 *Phys. Rev. Lett.* **71** 1993
[3] Chang Z, Rundquist A, Wang H, Murnane M M and Kapteyn H C 1997 *Phys. Rev. Lett.* **79** 2967
[4] Ivanov M, Corkum P B, Zuo T and Bandrauk A 1995 *Phys. Rev. Lett.* **74** 2933
[5] He L X, Zhu X S, Cao W, Lan P F and Lu P X 2022 *Chin. Phys. B* **31** 123301
[6] Liu J Q and Bian X B 2021 *Phys. Rev. Lett.* **127** 213901
[7] Ghimire S, DiChiara A D, Sistrunk E, Agostini P, DiMauro L F and Reis D A 2011 *Nat. Phys.* **7** 138
[8] Luu T T, Garg M, Kruchinin S Y, Moulet A, Hassan M T and Goulielmakis E 2015 *Nature* **521** 498
[9] Zhang Y F, Huang T F, Li J P, Yang K, Li L, Zhu X S, Lan P F and Lu P X 2021 *Chin. Phys. B* **30** 074204
[10] Guan Z, Liu L, Wang G L, Zhao S F, Jiao Z H and Zhou X X 2020 *Chin. Phys. B* **29** 104206
[11] Moiseyev N 2015 *Phys. Rev. A* **91** 053811
[12] Ndabashimiye G, Ghimire S, Wu M X, Browne D A, Schafer K J, Gaarde M B and Reis D A 2016 *Nature* **534** 520
[13] Wang S, Guo J W, He X K, Liang Y Y, Xie B C, Zhong S Y, Teng H and Wei Z Y 2023 *Chin. Phys. B* **32** 063301

[14] Du T Y, Huang X H and Bian X B 2018 *Phys. Rev. A* **97** 013403
[15] Yang Y, Lu J, Manjavacas A, Luk T S, Liu H, Kelley K, Maria J P, Runnerstrom E L, Sinclair M B, Ghimire S and Brener L 2019 *Nat. Phys.* **15** 1022
[16] Popovici C A, Ganeev R A, Vidal F and Ozaki T 2012 *J. Phys. B: At., Mol. Opt. Phys.* **45** 035601
[17] Peng D, Frolov M V, Pi L W and Starace A F 2018 *Phys. Rev. A* **97** 053414
[18] Qiao Y, Wang X Y, Li X F, Wu L Y, Yu R X, Guo F M, Wang J, Chen J G and Yang Y J 2023 *Opt. Express* **31** 36327
[19] Du J X, Wang G L, Gao X H, Li X Y, Jiao Z H, Zhao S F and Zhou X X 2024 *Opt. Lett.* **49** 061571
[20] Zou P, Zeng Z N, Zheng Y H, Lu Y Y, Liu P, Li R X and Xu Z Z 2010 *Phys. Rev. A* **81** 033428
[21] Du H C and Hu B T 2011 *Phys. Rev. A* **84** 023817
[22] Li P C, Zhou X X, Wang G L and Zhao Z X 2009 *Phys. Rev. A* **80** 053825
[23] Du T Y and Bian X B 2017 *Opt. Express* **25** 000151
[24] He L W, Yuan G L, Wang K, Hua W J, Yu C and Jin C 2019 *Photon. Research* **7** 001407
[25] Yue S J, Fu S L, Li J B, Zhang X, Feng Y K, Hu B T and Du H C 2018 *J. Chem. Phys.* **148** 234304
[26] Jia G R, Huang X H and Bian X B 2017 *Opt. Express* **25** 023654
[27] He L X, Zhang Q B, Lan P F, Cao W, Zhu X S, Zhai C Y, Wang F, Shi W J, Li M Z, Bian X B, Lu P X and Bandrauk A D 2018 *Nat. Commun.* **9** 1108
[28] Du H C, Xue S, Wang H Q, Zhang Z L and Hu B T 2015 *Phys. Rev. A* **91** 063844
[29] Pan X F, Li B, Huo X X, Zhang J and Liu X S 2021 *Laser. Phys.* **31** 025301
[30] Liu L, Zhao J, Yuan J M and Zhao Z X 2019 *Chin. Phys. B* **28** 114205
[31] He Y L, Guo J, Gao F Y, Yang Z J, Zhang S Q and Liu X S 2021 *Phys. Rev. A* **104** 013104
[32] Qiao Y, Chen J Q, Zhou S S, Chen J G, Jiang S C and Yang Y J 2024 *Chin. Phys. Lett.* **41** 014205
[33] Wang S, Liu S T, Huo X X, Xing Y H and Zhang J 2023 *Phys. Rev. A* **108** 063106
[34] Feng L Q and Chu T S 2011 *Phys. Rev. A* **84** 053853
[35] Carrera J J and Chu S I 2007 *Phys. Rev. A* **75** 033807
[36] Vampa G, McDonald C R, Orlando G, Corkum P B and Brabec T 2015 *Phys. Rev. B* **91** 064302
[37] McDonald C R, Vampa G, Corkum P B and Brabec T 2015 *Phys. Rev. A* **92** 033845
[38] Li J B, Zhang X, Fu S L, Feng Y K, Hu B T and Du H C 2019 *Phys. Rev. A* **100** 043404
[39] Mitrofanov A V, Sidorov-Biryukov D A, Glek P B, Rozhko M V, Stepanov E A, Shutov A D, Ryabchuk S V, Voronin A A, Fedotov A B and Zheltikov A M 2020 *Opt. Lett.* **45** 000750
[40] Song X H, Yang S D, Zuo R X, Meier T and Yang W F 2020 *Phys. Rev. A* **101** 033410
[41] Jia C, Wang J, Li Q Y, Guo F M, Chen J G, Zeng S L and Yang Y J 2015 *Opt. Express* **23** 032222
[42] Yu C, Iravani H and Madsen L B 2020 *Phys. Rev. A* **102** 033105
[43] Li J B, Fu S L, Wang H Q, Zhang X, Ding B W, Hu B T and Du H C 2018 *Phys. Rev. A* **98** 043409
[44] Bian X B and Bandrauk A D 2011 *Phys. Rev. A* **83** 041403
[45] Wang X Q, Liu M Q, Jia L J, Yan P G and Jiang W C 2023 *Phys. Rev. B* **108** 054306